Flying Qualities and Controllability of Hypersonic Spaceplanes

Mooij, Erwin; Viavattene, Giulia

DOI
10.2514/6.2019-1669

Publication date
2019

Document Version
Accepted author manuscript

Published in
AIAA Scitech 2019 Forum

Flying Qualities and Controllability of Hypersonic Spaceplanes

Gulia Viavattene* and Erwin Mooij†

Delft University of Technology, Faculty of Aerospace Engineering,

Kluyverweg 1, 2629 HS Delft, The Netherlands

The growing interest in hypersonic spaceplanes, as a new promising concept for space flight, requires that their flying qualities and controllability characteristics are well understood. These properties are investigated along a typical spaceplane's ascent and re-entry trajectory. The analyses of the stability, trim capabilities and flying qualities of the open-loop system should prove whether the spaceplane is dynamically stable. If not, a control system is required. A simple adaptive controller can be designed, focusing on the compromise between optimality and robustness. The current paper addresses the flying-quality and controllability analyses, together with the design of such a control system. The responses for both longitudinal and lateral control in nominal and off-nominal conditions are simulated and evaluated. This robust and advanced control system cannot only stabilise the vehicle with relatively low control effort, but also minimise the effect of disturbances on the overall performance, guaranteeing safety of flight and mission success.

Nomenclature

$\mathbf{A}$	state or system matrix, varies
$\mathbf{B}$	control input matrix, varies
$\mathbf{C}$	output matrix, varies
$\mathbf{e_y}$	output error, varies
f	function, varies
$\mathbf{I}$	inertia tensor, kgm^2
$\mathbf{K}$	control gain matrix (index e: output error, x: model state, u: model control), varies
$\mathcal{L}$,$\mathcal{M}$,$\mathcal{N}$	roll, pitch, yaw Moment, Nm
M	Mach number, -
M_T	propulsion moment, Nm
p, q, r	roll, pitch, yaw rate, rad/s
P	period, s
$\bar{q}$	dynamic pressure, Pa
$\mathbf{Q}$	weighting matrix (state deviation), varies
$\mathbf{R}$	weighting matrix (control effort), varies
t	time, s
$\mathbf{T}$	weighting matrix (adaptive gain), varies
$T_{1/2}$	time-to-halve the amplitude, s
$\mathbf{V}$	velocity, m/s
$\mathbf{x}$	state vector, varies

*MSc Graduate Student, Section of Astrodynamics and Space Missions, Delft University of Technology. Currently: PhD Student, g.viavattene.1@research.gla.ac.uk, University of Glasgow.

†Assistant Professor, Section of Astrodynamics and Space Missions, e.mooij@tudelft.nl, Associate Fellow AIAA.

$\mathbf{y}$	output vector, varies
α	angle of attack, rad
β	angle of sideslip, rad
$\Delta..$	deviation, varies
δ	deflection angle (index a: aileron, b: body flap, e: elevator, r: rudder, w: wing flap), rad
ϵ_T,ψ_T	thrust elevation and azimuth angles, rad
η	signal-to-noise ratio, dB
$\eta_{x,y,z}$	Commanded Moment Fractions, -
ζ	damping ratio, -
ρ	density, kg/m^3
σ	bank angle, rad
σ	standard deviation, varies
ω_n	natural frequency, rad/s

I. Introduction

The compliance of the vehicles with flying qualities and controllability characteristics is necessary to adequately perform the mission objectives and operate within the safety boundaries. *Flying qualities* involve the study and evaluation of the stability and control characteristics of a vehicle, with the purpose of ensuring flight safety and the ease of controlling the vehicle in both steady flight and during manoeuvres. The military documents MIL-F-8785[1] and MIL-HDBK-1797[2] define the flying-quality requirements for all categories of aircraft flying in the subsonic regime.

These requirements do not address the unique characteristics of hypersonic vehicles. The main differences with respect to conventional aircraft are a higher kinetic energy level, which causes a change in the interrelation between height and speed excursions during a perturbation, and an additional longitudinal mode of motion, the so-called *height mode*. Also, the long-term dynamic characteristics influence control and stability in a different way depending on the flight regime. Thus, it is essential to study and identify the flying qualities and the controllability characteristics of hypersonic vehicles.

Group III of large, heavy, low-to-medium manoeuvrability aircraft presents characteristics similar to those of hypersonic vehicles.[3] In that way, the flying qualities of hypersonic spaceplanes can be identified and compared with the military requirements. In case the specifications are not met, an advanced control system needs to be integrated into the system to stabilise and control it. The control system shall be designed to meet the MIL-requirements, taking into account the differences between subsonic and high-speed regimes. Amongst the advanced controllers, such as sliding mode, neural network, and reinforcement learning, simple adaptive control (SAC)[4] seems to be a promising a robust control concept for the current application.

SAC belongs to the family of the Model Reference Adaptive Control (MRAC) and it has been applied for attitude control of, for instance, robots,[5] single-stage-to-orbit spaceplanes,[6] and re-entry vehicles.[7] An optimal control-system design can be identified by minimising the performance metrics of the integrated control error and effort. Also, it is desirable that the control system is as insensitive to disturbances as possible. To this end, a double-loop sensitivity analysis process, also known as robust design methodology, can be set up and a robust control-system can be designed.

The layout of this paper is as follows. In Sec. II, the simulation model is described. It consists of the reference vehicle, which is a single-stage-to-orbit spaceplane, and the reference mission, i.e., the hypersonic ascent and re-entry trajectory with Mach number ranging from 5 to 20. To completely define the stability properties of the vehicle in nominal and off-nominal conditions, the characteristics of motion of the open-loop system shall be studied, together with the trimmability capabilities. Afterwards, the flying qualities can be identified and compared with the *MIL-Specs* requirements. These analyses are reported in Sec. III. Once it has been determined whether the vehicle is stable, the need for a control system arises. The control system is designed in Sec. IV. In Sec. V, the controllability analysis and the response to atmospheric disturbances are studied to investigate whether the control system is able to compensate for any deficiency of the system and meet the MIL specifications. These analyses will be conducted for some design points of the hypersonic ascent and re-entry trajectory. Finally, Sec. VI concludes this paper with some final remarks.

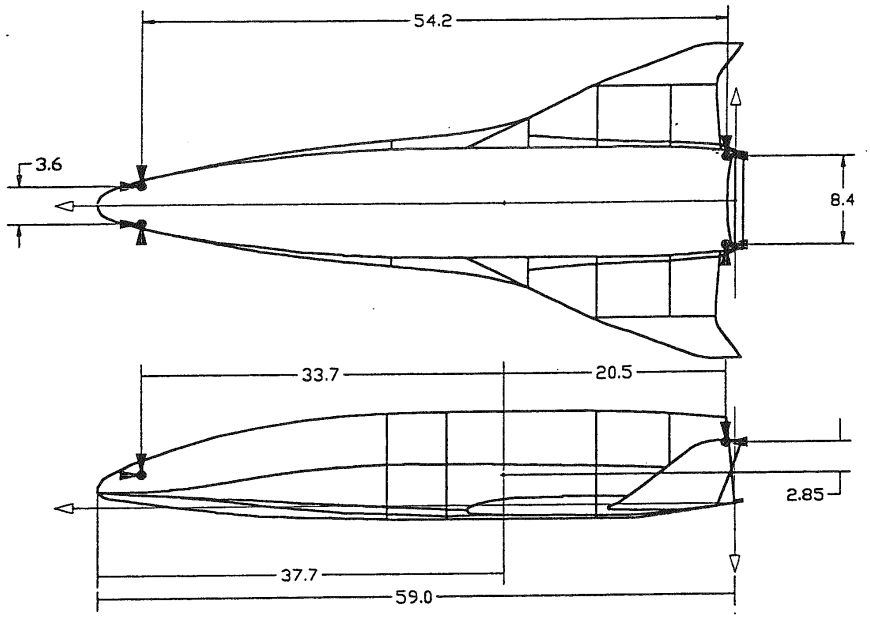

Figure 1: FSSC-1 reference vehicle.[8]

II. Simulation Model

A. Reference Vehicle and Mission

FESTIP System Study Concept 1 (FSSC-1) is one of the 16 vehicle concepts studied in the Future European Space Transportation Investigations Programme (FESTIP).[8] The vehicle is a vertical take-off, horizontal landing and single-stage-to-orbit with delta-shaped wings. This launch vehicle concept was derived from the HORUS configuration, which is the second stage of the TSTO launch vehicle Sänger II.[16] FSSC-1 is propelled by eight main rocket engines with a thrust level of 1800 kN. The ascent flight can be controlled by means of control surfaces, engine gimbal and throttle. It has a gross take-off weight of 900 tonnes and a fuselage length of 59 m. The mass model is defined assuming that the vehicle is a rigid structure and that, due to the use of its propulsion system, mass, the centre of mass (CoM) position and the inertia tensor change as a function of fuel consumption. Due to the close resemblance to HORUS, the aerodynamic model is fully defined and taken from the available database of HORUS. The propulsion model is defined based on values for thrust level, chamber pressure, specific impulse, oxidiser/fuel (O/F) mixture ratio, and nozzle expansion ratio.

Figure 1 illustrates the FSSC-1 reference vehicle. The vehicle performs a powered vertical take-off and ascent to orbit. The booster engine cut-off occurs at a height of 59 km, and main engine cut-off (MECO) at around 102 km altitude. Finally, after it has completed its orbital mission, it re-enters and lands horizontally after its hypersonic descent. It is chosen to investigate the stability and controllability characteristics in the points where the Mach number is 5, 10, 15, 20 along both the ascent and the re-entry trajectory. In this way a clear picture of the stability and controllability characteristics along the hypersonic trajectory can be drawn. The nominal conditions at each point of interest are presented in Table 2. Since no information about the bank angle along the ascent trajectory is offered, it is assumed to be zero. This is acceptable for this application, since we are more interested in the deviation between the actual and the desired attitude and how efficiently the system realises the commands to eliminate this deviation.

For the attitude control-system design, the rotational motion of the vehicle is studied. Since the products of inertia are much smaller than the moments of inertia, FSSC-1 can be considered to be rotational symmetric in mass. For this application, the state vector consists of the angular-rate components (roll rate p, pitch rate q, and yaw rate r), and the aerodynamic angles (angle of attack α, angle of sideslip β, and bank angle σ). For simulating the rotational dynamics, the full, non-linear model will be used. To design the control system,

Table 2: Nominal conditions at the design points along the ascent and re-entry trajectory.[8]

Initial Conditions	**Ascent**				**Re-entry**			
	M=5	**M=10**	**M=15**	**M=20**	**M=5**	**M=10**	**M=15**	**M=20**
Altitude [km]	34.54	64	79.85	91.27	35	46.9	59.03	68.84
Dynamic Pressure [Pa]	10,000	715	151	101	10,000	8000	4000	1900
Velocity [km/s]	1.53	3.07	4.22	5.48	1.54	3.29	4.73	5.96
Flight-path angle [°]	-3.31	-1.54	-0.38	-0.55	-3.32	-1.54	-0.38	-0.55
Angle of Attack [°]	3.77	4.31	4.39	2.96	11.82	14.08	18.12	28.76
Sideslip Angle [°]	0	0	0	0	0	0	0	0
Bank Angle [°]	0	0	0	0	57.81	-59.38	-29.80	59.42
Thrust [kN]	$14.7 \cdot 10^3$	$7.2 \cdot 10^3$	$7.2 \cdot 10^3$	$5 \cdot 10^3$	0			
Gross mass [kg]	$510 \cdot 10^3$	$340 \cdot 10^3$	$270 \cdot 10^3$	$180 \cdot 10^3$	$102 \cdot 10^3$			
$x^{\star}_{CoM}$ [m]	(35.6, 0, 2.8)	(36.6, 0, 2.8)	(36.7, 0, 2.8)	(36.8, 0, 2.8)	(37.7, 0, 2.8)			
I_{xx} [kg m^2]	$6646 \cdot 10^3$	$4878 \cdot 10^3$	$4187 \cdot 10^3$	$3320 \cdot 10^3$	$2489 \cdot 10^3$			
I_{yy} [kg m^2]	$81{,}680 \cdot 10^3$	$59{,}645 \cdot 10^3$	$51{,}012 \cdot 10^3$	$40{,}142 \cdot 10^3$	$29{,}115 \cdot 10^3$			
I_{zz} [kg m^2]	$82{,}351 \cdot 10^3$	$60{,}013 \cdot 10^3$	$51{,}262 \cdot 10^3$	$40{,}244 \cdot 10^3$	$29{,}123 \cdot 10^3$			
I_{xy} [kg m^2]	$-11 \cdot 10^3$	$-13 \cdot 10^3$	$-14 \cdot 10^3$	$-17 \cdot 10^3$	$-50 \cdot 10^3$			
I_{xz} [kg m^2]	$1 \cdot 10^3$	$1 \cdot 10^3$	$1 \cdot 10^3$	$0 \cdot 10^3$	$-10 \cdot 10^3$			
I_{zy} [kg m^2]	$5377 \cdot 10^3$	$3713 \cdot 10^3$	$3165 \cdot 10^3$	$2417 \cdot 10^3$	$1737 \cdot 10^3$			
$\star$ the CoM location is given with respect to the body reference frame.								

however, the longitudinal motion (defined by q and α) is commonly decoupled from the lateral motion (given by p, r, β and σ).

B. Actuators

The control surfaces of the reference vehicle are:

- left and right elevons: the deflection angles, respectively $\delta_{w,l}$ and $\delta_{w,r}$, are positive downward;
- left and right rudders: the deflection angles, respectively $\delta_{r,l}$ and $\delta_{r,r}$, are positive outward;
- body flap: the deflection angle, δ_b, is positive downward;

where the subscripts "r" and "l" are used to indicate the right and the left elevon/rudder, respectively. Note that the elevons provide the functions of both elevator (when symmetrically deflected) and aileron (when asymmetrically deflected). Thus, the elevator deflection, δ_e, is equal to the symmetric combination of the elevon deflections, while the aileron deflection, δ_a, is defined as the asymmetric combination of the two elevon deflections. The rudders can only be deflected outward, and therefore for yaw control only one rudder is active at a time.

Under normal operations, the vehicle is trimmed by the body flap and, when this does not suffice, it can be supported by the elevons and thrust elevation by gimbaling the engine nozzle. The longitudinal motion can be controlled by commanding the elevator, while the lateral motion can be controlled by commanding the aileron and rudder. Moreover, the main engines can be used to support the control surfaces in controlling the vehicle by changing the nozzle orientation so that the thrust vector points in the desired direction. This method is known as Thrust Vector Control (TVC). During re-entry, a similar contribution to attitude control is provided by the Reaction Control System (RCS).

During re-entry the control modes are set on the basis of the control scheme used for the Space Shuttle, which is shown in Fig. 2. It can be seen that when the dynamic pressure is too low for aerodynamic control, the reaction control thrusters are used. When the dynamic pressure has reached a sufficiently high value the control surfaces are activated. Following a period of hybrid control, in the final phase only aerodynamic control is used. During ascent, flown with small angle of attack, the control surfaces become inefficient for $\bar{q} < 5000$ Pa ($M > 5$) and TVC must be used to control the vehicle.

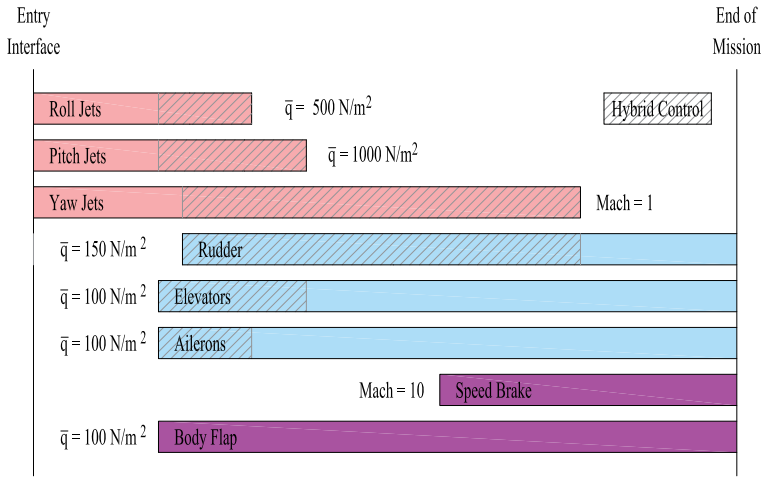

Figure 2: Control modes for FSSC-1 (and HORUS) during the re-entry flight.[11]

III. Stability and Flying-Quality Analysis

The analysis of the eigenmotion, also known as open-loop behaviour or free response of the system, corresponds to the study of the system's response to small perturbations of the state variables. Thus, only the homogeneous part of the linearised equations of motion written in state-space form, i.e., $\dot{\mathbf{x}} = \mathbf{A}\mathbf{x}$, is needed. The eigenmotion of the system can be analysed once the eigenvalues λ and eigenvectors $\boldsymbol{\mu}$ of the state matrix $\mathbf{A}$ are known.

The stability and periodicity of the motion can be examined by studying the eigenvalues. If an eigenvalue is a real number then the characteristic motion is aperiodic, while if it is complex the eigenmotion is periodic. The stability of the motion depends on the sign of the real part of the eigenvalues: when zero, the eigenmotion is indifferent, and when negative/positive, the eigenmotion is converging/diverging (*stable/unstable*).

Some coefficients need to be specified to characterise completely the motion of the system. For a converging motion, the time required to halve the amplitude of the deviation (*halving time*), $T_{\frac{1}{2}} = \frac{\ln \frac{1}{2}}{Re(\lambda)}$. For a periodic motion the *period* $P = \frac{2\pi}{Im(\lambda)}$, the *damping ratio* $\zeta = -\frac{Re(\lambda)}{\sqrt{Re(\lambda)^2+Im(\lambda)^2}}$, and the *natural frequency* $\omega_n = \sqrt{Re(\lambda)^2 + Im(\lambda)^2}$ are defined. The damping ratio is positive for converging motion, while it is negative for diverging motion.

The study of the eigenvectors offers a deeper insight in the characteristics of the eigenmotion. From the analysis of eigenvectors, it is possible to identify the components of the eigenmotion, that are known as *modes of motion*. In particular, the modulus and the argument of an eigenvector serve to comprehend, which of the state variables is involved in the motion and the phase difference between the involved state variables, respectively.

A. Eigenmotion

The characteristics of motion are generally different from conventional aircraft, due to the larger speed regime and the nature of the reference trajectory. One of the main differences is that it is possible to trace six modes of motion instead of five, being the *height mode* the additional mode for hypersonic vehicles. In addition, the modes of motion can present some differences with respect to subsonic aircraft. This analysis is conducted for four design points (Mach 5, 10, 15, 20) of the ascent and re-entry trajectory. Due to space limitations, not all results can be included; as an example the results for $M = 15$ along the ascent trajectory are provided in Table 3. The periodic modes that can be identified are the phugoid mode and the short-period mode. The driving components of the phugoid are the height and velocity, with almost negligible variation of the angle of attack that can be, consequently, considered constant. The short-period presents a large oscillation in angle of attack and pitch rate. It is different from the conventional short-period because the height and velocity might change, while they remain constant in subsonic regime. Moreover, its period is about 30 times larger, due to its larger speed regime.

Table 3: Eigenmotion analysis: ascent flight at Mach 15 (trimmed condition: $\epsilon_T = 0.15°$).

Mach 15									
$\boldsymbol{\lambda_i}$	**Phugoid**		**Short period oscillation**		**Height mode**	**Aperiodic lateral mode**		**Roll mode**	
$\mathrm{Re}(\lambda_i)$	-0.4078		0.2801		$0.6786 \cdot 10^{-5}$	0.6284	-0.6322	0.0684	≈ 0
$\mathrm{Im}(\lambda_i)$	$\pm$0.2258		0.0875		-	-	-	-	-
P [s]	71.78		27.83		-	-	-	-	-
$T_{1/2}$ [s]	1.70						1.09		
T_2 [s]			2.48		70826.3	1.11		10.14	$3.1 \cdot 10^{15}$
ζ [-]	0.9777		-0.7784		-	-	-	-	-
ω_n [rad/s]	0.4171		0.3597		-	-	-	-	-
$\boldsymbol{\mu_i}$	z [-]	θ [°]	z [-]	θ [°]	z [-]	z [-]	z [-]	z [-]	z [-]
Δ_V	**0.0769**	**161.65**	**0.0957**	**157.26**	$0.2094 \cdot 10^{-5}$	0	0	0	0
Δ_γ	$0.4158 \cdot 10^{-6}$	166.14	$0.4064 \cdot 10^{-6}$	37.66	$0.9610 \cdot 10^{-7}$	0	0	0	0
Δ_R	**1.0000**	**0**	**1.0000**	**0**	**1.0000**	0	0	0	0
Δ_p	0	0.46	0	26.73	0	**0.2710**	**0.2910**	$0.3585 \cdot 10^{-2}$	$0.8198 \cdot 10^{-2}$
Δ_q	$0.1326 \cdot 10^{-8}$	129.60	$\mathbf{0.1543 \cdot 10^{-2}}$	**104.12**	0	0	0	0	0
Δ_r	0	34.54	0	73.93	0	**0.4410**	**0.4735**	**0.0952**	**0.0902**
Δ_α	$0.4456 \cdot 10^{-6}$	28.98	$\mathbf{0.3185 \cdot 10^{-2}}$	**87.61**	$0.6639 \cdot 10^{-7}$	0	0	0	0
Δ_β	0	137.58	0	89.25	0	**0.6523**	**0.7045**	**0.0153**	0
Δ_σ	0	0	0	156.84	0	**0.5538**	**0.4413**	**1.0000**	**1.0000**

All the other modes are aperiodic. Some of them presents the same characteristics of the height modes, identified for the first time while studying stability in hypersonic flight.[17] One is unstable and lightly amplified. The remaining two have both the height and velocity as dominating components, thus they are named as *height & velocity modes* to distinguish them from the pure height mode. One height & velocity mode is stable, whereas the other one is unstable, exhibiting rapid convergence and divergence, respectively. It is notable that it can happen that more than one of the same characteristic motion is present, due to a degeneration of a complex mode ino two separate aperiodic modes. The remaining modes are two aperiodic lateral modes and two aperiodic roll modes. The former have the angle of sideslip, bank angle, and the corresponding angular rates as main components. The latter are dominated by the bank angle, as its name suggests. One of these modes presents a larger sideslip angle with respect to the other one, thus it can be compared with the roll convergence of conventional aircraft.

If the evolution of the eigenvalues and eigenvectors in time are studied, it can be noticed that the phugoid is a stable motion and remains to be so. The damping ratio increases, becoming a well-damped motion with $T_{1/2}$ decreasing from 460 s to 1.7 s. Simultaneously, the period decreases in time, going from around 1330 s at Mach 5 to 570 s at Mach 10 and arriving at 72 s at Mach 15. From Mach 15 to 20, the periodic phugoid mode breaks into two aperiodic modes, both stable and highly damped ($T_{1/2} = 0.7$ s). In these two modes the influence of the angle of attack and pitch rate becomes more important, increasing four orders of magnitude. For this reason, they could seem to be height & velocity modes, but the higher influence of Δq leads to define them as *pitch convergence modes*.

The height and velocity modes are two aperiodic modes, of which one is strongly damped ($T_{1/2} = 3.8$ s) and the other one is strongly diverging ($T_2 = 3.7$ s). The times to half/double-the-amplitude decreases in time, meaning that the stable (unstable) modes become more stable (unstable). At Mach 15, these two aperiodic modes combine into one periodic mode, the short-period mode, which is unstable with T_2 of 2.5 s at $M = 15$ and 3.3 s at $M = 20$. The height mode is an aperiodic mode, which is initially unstable with T_2 = 505 s at Mach 5. It becomes less unstable in time, reaching a T_2 in the order of about 10^5 s at Mach 15 and, finally, it turns into a stable mode at $M = 20$.

The aperiodic lateral motion presents two modes, one stable and one unstable. At Mach 5 strong convergence of the stable mode and strong divergence of the unstable mode are induced. In time the stable and unstable components become more emphasised, which is a confirmation that the system is not improving its lateral stability properties. A similar situation is experienced for the aperiodic roll motion, which is degenerated into two roll modes. One is unstable with a T_2 that is decreasing over time, but at Mach 20 it starts to grow. The other mode is stable, but it is characterised by a large value of T_2 of order $\sim 10^{15}$ s and could be considered indifferent.

The analysis of eigenmotion of FSSC-1 along the re-entry trajectory is similarly conducted. It results

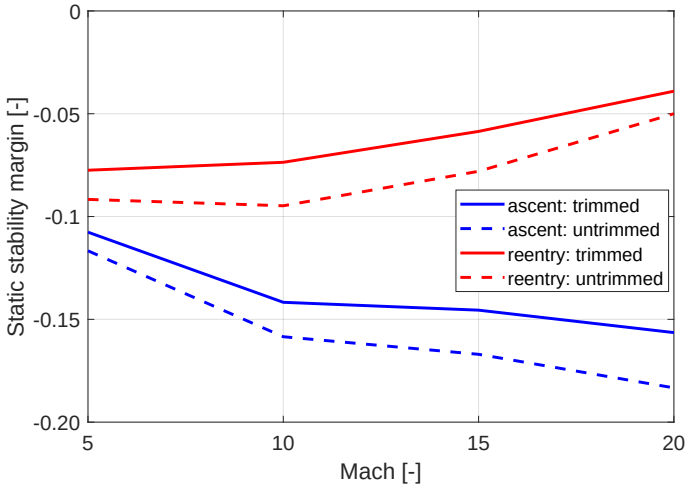

Figure 3: Static stability margin as function of Mach number (calculated at M = 5,10,15,20).

that the periodic modes are unstable, while the aperiodic mode experienced are described by two separated modes, one unstable and one stable, the latter being the predominant one. Over time, the periodic modes become less unstable with increasing time-to-double the amplitude, but without reaching a stable condition. It is interesting to notice that, being FSSC-1 derived from the HORUS configuration, it presents similar characteristics to the HORUS eigenmotion along the re-entry trajectory.[18]

It can be concluded that the vehicle is not stable in either its ascent or re-entry flight. Although in the following section it is investigated how trimming the vehicle can improve stability, this analysis confirms that the vehicle needs to be actively controlled.

B. Trim Analysis

A trim analysis is conducted for the ascent and re-entry trajectory. As mentioned before, the trim is provided by the body flap with the support of the elevator. However, it has been found that along the ascent for Mach>5 the effectiveness of the control surfaces reduces drastically with decreasing dynamic pressure, until it cannot provide any convenient contribution to trim for $\bar{q} \leq 5000$ Pa. Thus, above Mach 5 the need for thrust vectoring for trim arises.

A measure that is essential to quantify the stability and the controllability of aircraft is the *static stability margin*. It evaluates the non-dimensional distance between the CoM and the neutral point, expressed in percentage of the reference length: $\frac{x_N}{L_{ref}} = -\frac{C_{m\alpha}}{C_{L\alpha}}$. The vehicle is stable when the static margin is positive, i.e., $-\frac{C_{m\alpha}}{C_{L\alpha}} > 0$. It is shown in Fig. 3 that the static margin along the ascent trajectory suggests instabilities for $M \geq 5$. Indeed, the $C_{m\alpha}$ slope is positive for hypersonic Mach numbers and the range of angle of attack that is of interest for the hypersonic ascent flight ($2.5° \leq \alpha \leq 5°$). In addition, with increasing Mach number the $C_{L\alpha}$ slope reduces, driving the static margin to values indicating instability.

Along the re-entry trajectory the vehicle can be trimmed by using the body flap and, if not sufficient, aided by the elevator. Figure 3 describes the variation of the static margin as function of Mach along the re-entry trajectory. It shows instability along the whole re-entry flight, becoming more unstable towards the end of the hypersonic descent. The difference with respect to the ascent trajectory is mainly linked to the different ranges of angle of attack for the relevant parts of the flight. Indeed, along the re-entry the angle of attack goes from about 30° at $M = 20$ to 12° at $M = 5$, for which the $C_{m\alpha}$ slope decreases. It is concluded that trim reduces the instability of the system, but not enough to make the vehicle stable.

C. Flying Qualities

The FSSC-1 flying qualities are studied by comparing them with the set of military specifications[1,2] Given the different characteristics of the eigenmotion with respect to conventional aircraft, only the requirements applicable for our system are considered.

Table 4: Phugoid requirements.[2]

Phugoid	
Level 1	$\zeta_{ph} \geq 0.04$
Level 2	$\zeta_{ph} \geq 0$
Level 3	$T_{2_{ph}} \geq 55$ s

Table 5: Short-period requirements.[2]

Short Period	
Level 1	$0.30 \leq \zeta_{sp} \leq 2.00$
Level 2	$0.20 \leq \zeta_{sp} \leq 2.00$
Level 3	$0.15^{\star} \leq \zeta_{sp}$

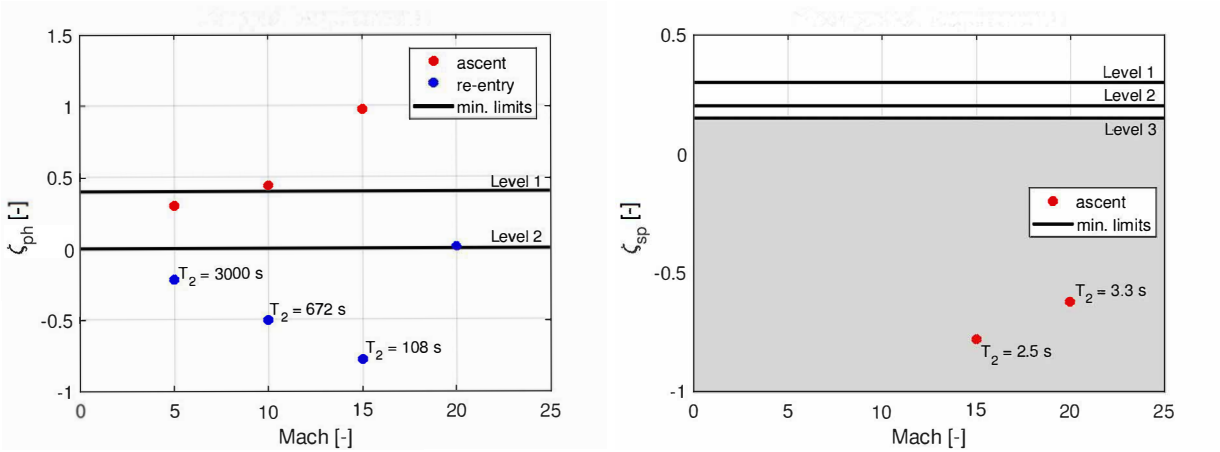

Figure 4: Phugoid (left) and short-period (right) requirements[2] and FSSC-1 characteristics of motion.

Table 6: Lateral oscillations: requirements[2] and FSSC-1 characteristics of motion.

Lateral Oscillation			
	ζ_{n_d} [-]	$\zeta_{n_d}\omega_{n_d}$ [rad/s]	ω_{n_d} [rad/s]
Level 1	$\zeta_{n_d} \geq 0.08$	$\zeta_{n_d}\omega_{n_d} \geq 0.15$	$\omega_{n_d} \geq 0.4$
Level 2	$\zeta_{n_d} \geq 0.02$	$\zeta_{n_d}\omega_{n_d} \geq 0.05$	$\omega_{n_d} \geq 0.4$
Level 3	$\zeta_{n_d} \geq 0$	Not specified	$\omega_{n_d} \geq 0.4$
FSSC-1 Characteristics (re-entry)			
Mach 15	-0.06	-0.02	0.36
Mach 20	-0.005	-0.007	1.29

Tables 4 and 5 define the requirements of the phugoid and short-period oscillation and Fig. 4 illustrates the FSSC-1 characteristics of motion. The phugoid is a stable motion during ascent, achieving Level 2 at Mach 5, but reaching Level 1 from Mach 10 onwards; this confirms what was found during the eigenmotion analysis. Differently, during re-entry the phugoid is characterised by negative damping ratios, indicating an unstable mode. It achieves Level 2 at Mach 20, then it deteriorates at Mach 15 and improves again down to Mach 5. However, Level 3, which is given in terms of time-to-double the amplitude, is assured if $T_2 \geq 55$ s, thus it is met. So, the phugoid satisfies Level 1 along the ascent and Level 3 along the re-entry trajectory. The short-period oscillation is experienced only in the last portion of the ascent flight, where it does not meet the requirements, as shown in Fig. 4 on the right.

The last periodic mode is the lateral mode. This is experienced only in the initial phase of the re-entry flight. Table 6 describes the requirements and the relative characteristics of the FSSC-1 motion. Two out of three requirements are not met, thus it is concluded that the lateral mode is not in compliance with the MIL-Specs. In conclusion, the vehicle is unstable and it needs to be controlled to perform a stable flight and achieve the mission objectives.

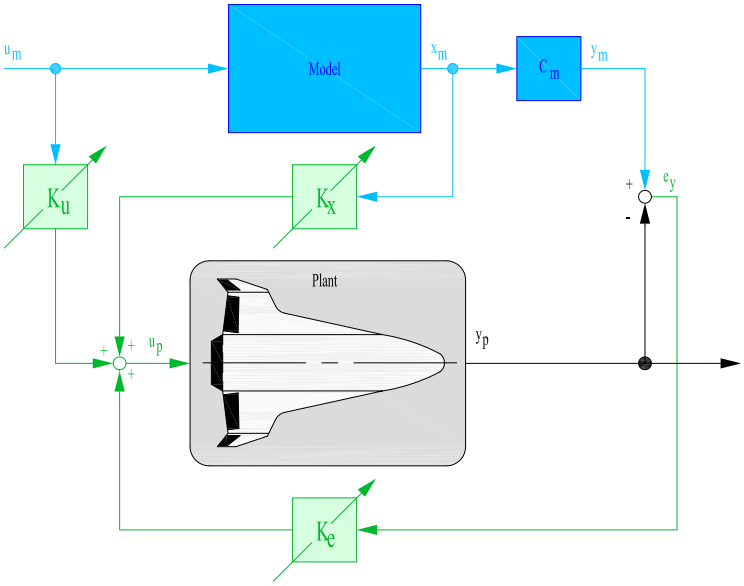

Figure 5: Simple adaptive control system: simplified model.[10]

IV. Simple Adaptive Control

A. Background

In this section a brief overview of the mathematical model of the SAC is offered, based on Ref. 4. This controller is based on the concept of *model following*, i.e., matching the response of the plant, which is the system to be controlled, to the response of a reference model.

Here, the reference model is described by a set of linearised state-space models[a]:

$$\dot{\mathbf{x}}_\mathbf{m} = \mathbf{A}_\mathbf{m}\mathbf{x}_\mathbf{m} + \mathbf{B}_\mathbf{m}\mathbf{u}_\mathbf{m} \tag{1}$$

where $\mathbf{x_m}$ is the $n \times 1$ model state vector, $\mathbf{u_m}$ is the $m \times 1$ model control vector, and $\mathbf{A_m}$ and $\mathbf{B_m}$ the $n \times n$ model state matrix and $n \times m$ model control matrix, respectively. Similarly, the output equation is:

$$\mathbf{y}_\mathbf{m} = \mathbf{C}_\mathbf{m}\mathbf{x}_\mathbf{m} \tag{2}$$

where $\mathbf{y_m}$ is the $q \times 1$ model output vector and $\mathbf{C_m}$ is the $q \times n$ model output matrix. The subscript m is added to distinguish the variables from the corresponding plant ones.

Differently, the *plant* is described by the following set of non-linear differential equation:

$$\dot{\mathbf{x}}_\mathbf{p} = \mathbf{f}(t, \mathbf{x}_\mathbf{p}, \mathbf{u}_\mathbf{p}) \tag{3}$$

$$\mathbf{y}_\mathbf{p} = \mathbf{g}(\mathbf{x}_\mathbf{p}, \mathbf{u}_\mathbf{p}) \tag{4}$$

where $\mathbf{x_p}$ is the $n_p \times 1$ plant state vector, $\mathbf{u_p}$ is the $m \times 1$ plant control vector, $\mathbf{y_p}$ is the $q \times 1$ plant output vector, $\mathbf{f}$ and $\mathbf{g}$ are the $n_p \times 1$ and $q \times 1$ plant vector functions. The subscript p is added to the variables to underline the fact that this set of equations describes the behaviour of the non-linear plant.

Figure 5 shows a simplified scheme of the SAC. It is shown that the inputs to the plant are the model input $\mathbf{u_m}$, the model state $\mathbf{x_m}$, and the output error $\mathbf{e_y}$, which is the difference between the model output and the plant output. The inputs to the plant are obtained by multiplying these variables $\mathbf{u_m}$, $\mathbf{x_m}$, and $\mathbf{e_y}$ with the adaptive gains, which are $\mathbf{K_u}$, $\mathbf{K_x}$, and $\mathbf{K_e}$, respectively. These gains are adaptive in the sense that they vary with time, adapting their values to the changing conditions and leading to an improvement of the

[a]As the plant is following the model, it is important to give the model the required stability – and controllability – properties. In this situation this means that the model is stabilised by a simple feedback control system, where the gains are determined using optimal control theory. Such a controller is known as a Linear Quadratic Regulator (LQR).

robustness and stability of the system. Thus, also $\mathbf{K_u}(t)$, $\mathbf{K_x}(t)$, and $\mathbf{K_e}(t)$ are a function of time, but for the sake of convenience the "(t)" is dropped.

The control law of the adaptive-control algorithm is:

$$\mathbf{u_p} = \mathbf{K_r r} \tag{5}$$

where $\mathbf{r}$ is the vector of the three measurable signals and $\mathbf{K_r}$ the matrix combining the adaptive gains:

$$\mathbf{r} = (\mathbf{e_y}, \mathbf{x_m}, \mathbf{u_m})^T, \quad \mathbf{K_r} = [\mathbf{K_e}, \mathbf{K_x}, \mathbf{K_u}] \tag{6}$$

The adaptive gains are calculated by defining $\mathbf{K_r}$ as the sum of an integral and a proportional component:

$$\mathbf{K_r} = \mathbf{K_i} + \mathbf{K_p} \tag{7}$$

with

$$\dot{\mathbf{K}}_\mathbf{i} = \mathbf{e_y r}^T \mathbf{T_i}, \quad \mathbf{K_p} = \mathbf{e_y r}^T \mathbf{T_p} \tag{8}$$

where the weighting matrices $\mathbf{T_i}$ and $\mathbf{T_p}$ are positive definite and positive semi-definite, respectively.

Finally, the damping of the system can be improved by expressing the output error $\mathbf{e_y}$ as a linear combination of the state variables:

$$\mathbf{e_y} = \mathbf{y_m} - \mathbf{y_p} = \mathbf{K_{lqr,c}}(\mathbf{C_m x_m} - \mathbf{C_p x_p}) \tag{9}$$

where the output matrix is adjusted by pre-multiplying it with the optimal control-gain matrix, $\mathbf{K_{lqr,c}}$, that is also used to stabilise the reference model.

The adaptive control is possible when the adaptive system is state and gain bounded and presents an asymptotically stable output error. So, the plant is required to be *almost strictly passive* (ASP). Determining whether a plant is ASP is not so trivial. However, when the external moments are directly commanded, instead of the control actuators, the system is ASP.[11] This does not only make the system ASP, but also makes the controller independent of the operational conditions. Indeed, the moments are assigned to the actuators *outside* the controller. Moreover, since the maximum available moments differ along the trajectory depending on the flight conditions, the moment fractions of the maximum available moments are chosen as control variables. In this way, the control system design is facilitated and valid for all the flight conditions.

The moment factions are identified with η_x, η_y, and η_z and can vary between -1 and $+1$. So, the adaptive controller is composed by three controllers for roll, pitch, and yaw. Each controller is characterised by a different output error e_y (which is a scalar for each controller), model state vector $\mathbf{x_m}$ and control vector $\mathbf{u_m}$. In particular, for roll and yaw control, the weighting matrices $\mathbf{T_i}$ and $\mathbf{T_p}$ have dimensions 6×6 with $\mathbf{r} = (e_x\ p_m\ r_m\ \beta_m\ \sigma_m\ \eta_{x,m})^T$ and $\mathbf{r} = (e_z\ p_m\ r_m\ \beta_m\ \sigma_m\ \eta_{z,m})^T$, respectively. For pitch control, $\mathbf{T_i}$ and $\mathbf{T_p}$ have dimensions 4×4 with $\mathbf{r} = (e_y\ q_m\ \alpha_m\ \eta_{y,m})^T$. These definitions help to show how the control output around an axis is directly related to the corresponding control error.

B. Reference Model

As mentioned, the reference model is represented by a sequence of state-space nmodels covering the complete flight range, and stabilised by a linear state-feedback controller, the LQR. The model considers decoupled longitudinal and lateral motion, and the control gains are computed by means of optimal control theory.[12] The reference model is designed such that the system's performance requirements enter the design.

The (discretised) reference model should run at a frequency of 25 Hz to remain stable at higher dynamic pressure.[10] The weighting matrices $\mathbf{Q}$ and $\mathbf{R}$ of maximum state deviation and control effort, respectively, are defined, using *Bryson's Rule*, by the maximum allowable error in the commanded attitude, and the maximum control moment-fractions. If smaller allowable error are specified, the reference-model response, which the plant will follow by properly tuning the adaptive gains, will be faster.

Along the re-entry trajectory, the maximum allowed amplitudes of the state variables are $\Delta\alpha_{max} = 1°$, $\Delta\beta_{max} = \Delta\sigma_{max} = 2°$, and $\Delta p_{max} = \Delta q_{max} = \Delta r_{max} = 10°/\text{s}$, and of the control variables are $\Delta\eta_{x,max} = \Delta\eta_{y,max} = \Delta\eta_{z,max} = 1$. Along the ascent trajectory, these values of allowable rotational-rate errors lead to slower response, so they need to be decreased. In this way, the control is tighter and, consequently, the response faster. So, the maximum allowable state error are now determined: $\Delta\alpha_{max} = 1°$, $\Delta\beta_{max} = \Delta\sigma_{max} = 2°$, and $\Delta p_{max} = \Delta q_{max} = \Delta r_{max} = 4°/\text{s}$.

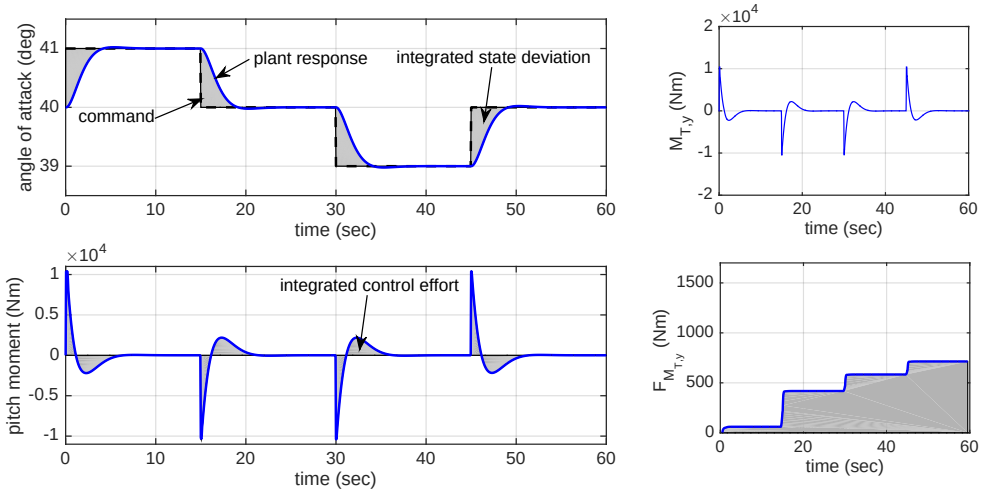

Figure 6: Graphical representation of the controller performance indices.[10]

C. Baseline Control Design

The performance of the controller can be evaluated by means of objective functions to minimise the state deviation between the plant and the control commands and to minimise the control effort. It follows that the integrated control error and the integrated control effort can give information about the performance of the control action and about how optimal it is.

For the longitudinal control system design, the two objectives are expressed as:

$$\sum_{\alpha_{err}} = \int_0^t |\alpha_c(t) - \alpha_p(t)|\mathrm{d}t \qquad \sum_{\eta_y} = \int_0^t |\eta_y(t)|\mathrm{d}t \tag{10}$$

For the lateral control system design, the objective functions can expressed as:

$$\sum_{\sigma_{err}} = \int_0^t |\sigma_c(t) - \sigma_p(t)|\mathrm{d}t \qquad \sum_{\eta_x} = \int_0^t |\eta_x(t)|\mathrm{d}t \qquad \sum_{\eta_z} = \int_0^t |\eta_z(t)|\mathrm{d}t \tag{11}$$

Also, it is desirable that the actuator commands refrain from oscillations. Thus, a cumulative moving standard deviation is used to measure the oscillations or any discrete changes in the controls. The gradient of the cumulative standard deviation measures the local oscillations as follows:

$$\sum_{F_{u_j}} = \int_0^t |F_{u_j}(t)|\mathrm{d}t \tag{12}$$

where the signal u can be the activity of any of control variables. This measure should be as small as possible for smoother control. It should be noticed that this index is only indicative, because it depends on the dimension of the sample interval chosen and the mean-control-value progression. However, it is functional for the optimisation of the controller.

Figure 6 provides a graphical representation of the above indices, which are represented by the gray areas, for a sequence of angle-of-attack step commands during the HORUS re-entry flight when only reaction control is available. On the right of this figure, a graphical representation of the integrated actuator oscillations is provided, where it is shown that the jumps in control moment lead to a rapid increase of $\sum_{F_{M_{T,y}}}$. Thus, to define the baseline control-system design a Monte Carlo simulation (N= 1000) is performed, so that the design with the minimum performance indices is identified.

The performance of the response to an angle-of-attack step command is examined at $M = 15$ in both the ascent and re-entry trajectory. For the sake of brevity, only the performance of the controller along the re-entry trajectory is presented in Fig. 7. In the given examples the performance indices are for the

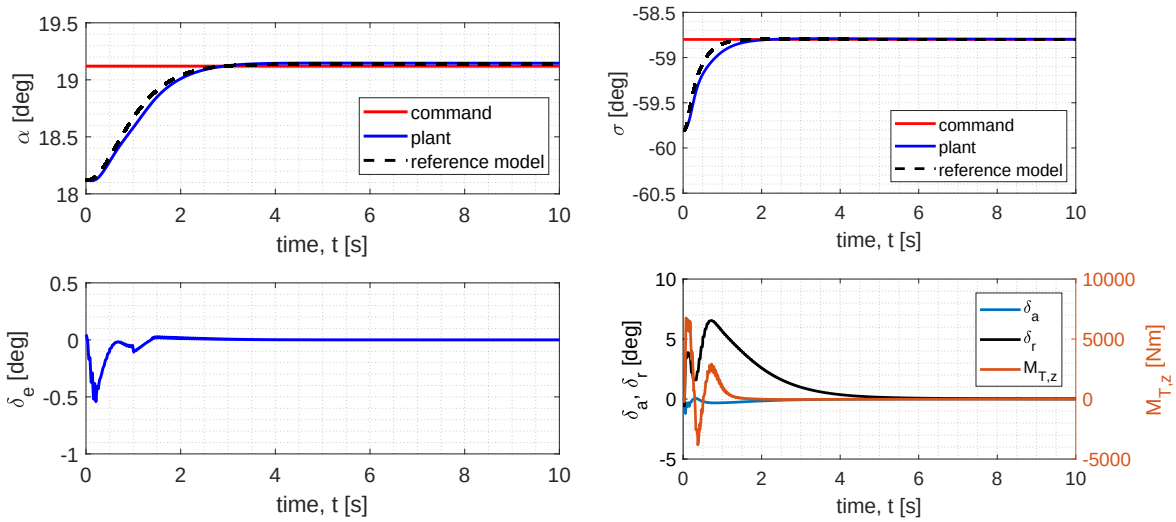

Figure 7: *Baseline design*: control error and control effort for an angle-of-attack (left) and bank-angle (right) step command at design point with $M = 15$ along the re-entry trajectory.

angle-of-attack command:

$$\text{for ascent:} \quad \sum_{\alpha_{err}} = 278.9°\text{s} \qquad \sum_{\eta_y} = 14.4\ \text{s} \qquad \sum_{F_{\eta_y}} = 0.3\ \text{s} \tag{13}$$

$$\text{for re-entry:} \quad \sum_{\alpha_{err}} = 266.1°\text{s} \qquad \sum_{\eta_y} = 3.0\ \text{s} \qquad \sum_{F_{\eta_y}} = 0.4\ \text{s} \tag{14}$$

and for the bank-angle command:

$$\text{for ascent:} \quad \begin{cases} \sum_{\sigma_{err}} = 289.6°\text{s} & \sum_{\eta_x} = 15.5\ \text{s} \quad \sum_{\eta_z} = 5.6\ \text{s} \\ \sum_{F_{\eta_x}} = 0.7\ \text{s} & \sum_{F_{\eta_z}} = 0.5\ \text{s} \end{cases} \tag{15}$$

$$\text{for re-entry:} \quad \begin{cases} \sum_{\sigma_{err}} = 233.4°\text{s} & \sum_{\eta_x} = 5.4\ \text{s} \quad \sum_{\eta_z} = 16.8\ \text{s} \\ \sum_{F_{\eta_x}} = 0.2\ \text{s} & \sum_{F_{\eta_z}} = 0.5\ \text{s} \end{cases} \tag{16}$$

D. Robust Control Design

The control system is designed to control the vehicle along its reference trajectory, even if deviations from the nominal conditions can occur due to uncertainties in initial conditions, atmospheric status and vehicle parameters. Thus, it is desirable that the control system is able to control the FSSC-1 vehicle and realise the input commands even in the presence of design uncertainties. Although these perturbations cannot be predicted, the control system has to be able to minimise their effects on the system so that the nominal trajectory can be flown. A control system with these characteristics is said to be *robust* with respect to disturbances.

A *robust design* methodology is applied. It is a technique defined as an "engineering methodology for improving productivity during research and development so that high-quality products can be produced quickly and at low cost".[15] The concept behind robust design is to improve the quality of the product by minimising the effect of the cause of variation without eliminating the cause. The response of the control system can be influenced by three classes of parameters: the *signal factors*, which are set by the user, expressing the intended value for the product's response; the *noise factors* that cannot be controlled by the designer; and the *control factors* that can be specified freely by the designer.

One of the major tools that can be exploited in robust design is the *signal-to-noise ratio* (SNR), which

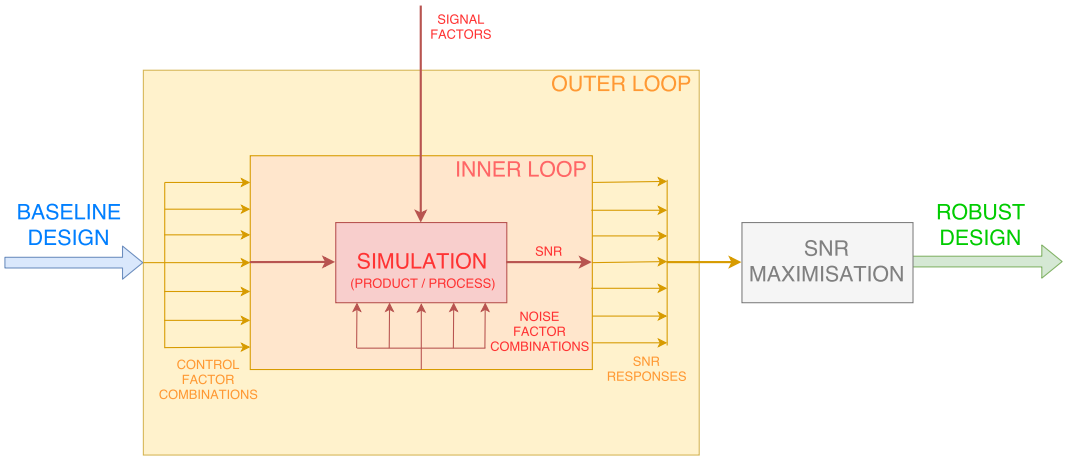

Figure 8: Robust design process.

is a measure of the quality of the product. The SNR is measured in decibels (dB) and is defined as follows:

$$\eta = 10 \log_{10} \left(\frac{\bar{y}^2}{\sigma^2} \right) \tag{17}$$

with $\bar{y}$ being the mean value of the response or, in other words, the desirable value, and σ being the standard deviation that quantifies the effect of the noise factors. The most robust design is the one characterised by the maximum value of SNR, which corresponds to minimising the sensitivity to noise factors, by either increasing the nominal performance $\bar{y}$, or by reducing the standard deviation σ. To study the robustness of the control system of the FSSC-1, the SNR of the performance metrics of the integrated control error and effort will be exploited.

To identify the robust design of the SAC control system for the FSSC-1 reference vehicle, a double-loop sensitivity analysis is designed. A schematic representation of the robust design process is illustrated in Fig. 8. The sensitivity analyses involve two design loops: in the outer loop the control factors are varied around the baseline design, while in the inner loop the noise factors are varied. Thus, for each control-factor combination identified in the outer loop, a sensitivity analysis is conducted in the inner loop for all the noise-factor combinations, with a signal-to-noise ratio as outcome. At the end of the simulation, a number of signal-to-noise ratios equal to the number of outer-loop combinations is available. The *robust design* results to be that combination of control design parameters that is characterised by the maximum signal-to-noise ratio.

The weighting matrix coefficients $\mathbf{T_i}$ and $\mathbf{T_p}$ are varied by a range of $\pm 50\%$. The noise factors are varied in the inner loop with respect to their nominal values. They are the initial conditions, p_0, r_0, q_0, α_0, β_0, σ_0, the mass and inertia properties, m, $\mathbf{I}$, the atmospheric property, ρ, and the aerodynamic coefficients, C_D, C_S, C_L, C_l, C_m, and C_n. Since the characteristics of the FSSC-1 are identified graphically and the aerodynamic coefficients are obtained by correcting the HORUS aerodynamic database, the uncertainty of the noise factors could be quite high. For this reason, it is assumed that the noise factors can be subjected to perturbation from $\pm 10\%$ to $\pm 50\%$ of their nominal value, to consider both the best case and worst case scenario.

The sensitivity analysis is implemented so that $N_{outer} = 500$ simulations for outer loop and $N_{inner} = 500$ for the inner loop. The results are generated by initialising the random number generator (RNG) with the same seed at every simulation batch, so that it is possible to reproduce the noise-factor variations for each combination of control factors. In this way, it can be ensured that the design space is entirely covered and it is possible to obtain statistically relevant results. Also, two batches of simulations are performed: one for $\pm 10\%$ and one for $\pm 50\%$ variation of the noise factors.

The results show that an improvement in terms of robustness is possible with respect to the optimal baseline design for both the longitudinal and lateral motion. In particular, a combination of design parameters is found to be robust with respect to both moderate uncertainties and severe uncertainties of the noise factors, so that the controller is able to realise the commands even for the worst-case combination of perturbations.

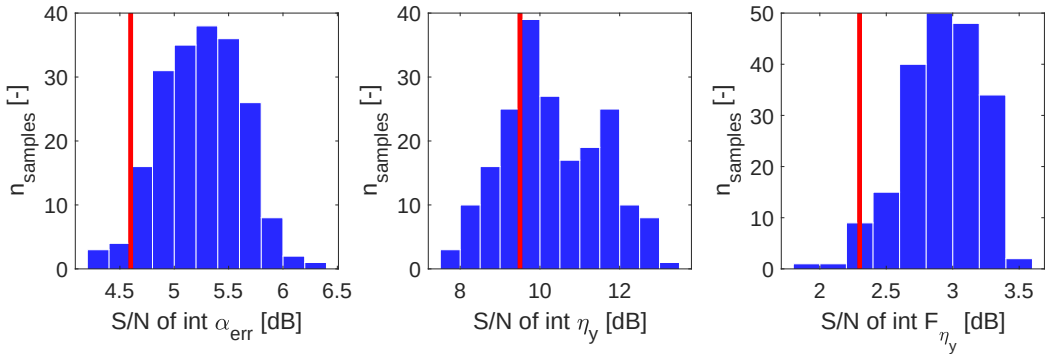

Figure 9: Performance index SNR due to uniform variation ($\pm$ 50%) of the noise factors to realise an α command at $M = 15$ of the re-entry trajectory. The red line represents the baseline design.

Table 7: Performance at $M = 15$ during re-entry: comparison between baseline and robust design.

Longitudinal Motion			**Lateral Motion**		
Perf. Indices	*Baseline Design*	*Robust Design*	*Perf. Indices*	*Baseline Design*	*Robust Design*
$\sum_{\alpha_{err}}$	266.1°s	340.3°s	$\sum_{\sigma_{err}}$	233.4°s	237.2°s
$\sum_{\eta_y}$	3.0 s	1.9 s	$\sum_{\eta_x}$	5.4 s	5.2 s
$\sum_{F_{\eta_y}}$	0.4 s	0.6 s	$\sum_{\eta_z}$	16.8 s	16.9 s
			$\sum_{F_{\eta_x}}$	0.2 s	0.3 s
			$\sum_{F_{\eta_z}}$	0.5 s	0.5 s
SNR	*Baseline Design*	*Robust Design*	*SNR*	*Baseline Design*	*Robust Design*
$\eta_{\sum_{\alpha_{err}}}$	4.5 dB	6.3 dB	$\eta_{\sum_{\sigma_{err}}}$	1.9 dB	2.5 dB
$\eta_{\sum_{\eta_y}}$	9.5 dB	12.8 dB	$\eta_{\sum_{\eta_x}}$	6.2 dB	7.3 dB
$\eta_{\sum_{F_{\eta_y}}}$	2.3 dB	3.5 dB	$\eta_{\sum_{\eta_z}}$	2.6 dB	3.9 dB
			$\eta_{\sum_{F_{\eta_x}}}$	1.7 dB	3.2 dB
			$\eta_{\sum_{F_{\eta_z}}}$	0.3 dB	0.5 dB

Due to space limitations, only a single example of the results is presented by the histogram plots of the batch of simulations with $\pm$50% variation of the noise factors (Fig. 9) for the re-entry flight ($M = 15$), when an angle-of-attack step is commanded. Analogous analyses are performed for the lateral motion and in the other design points of the trajectory.

The larger margin of improvement is provided by the SNR of the integrated oscillations of the control variables. The SNR values of the performance indices are maximised with respect to those of the optimal design (as it is mainly driven by the standard deviation), while showing still an excellent performance in terms of integrated control error and effort, as shown in Table 7. Comparing the baseline design with the robust design shows that, overall, the coefficients that are increased more are those related to $\mathbf{e_y}$, α_m, σ_m, and $\boldsymbol{\eta_m}$. Indeed, SAC is based on a model-following scheme, for which the plant should realise the command by following the model response and activating the actuators similarly to the model.

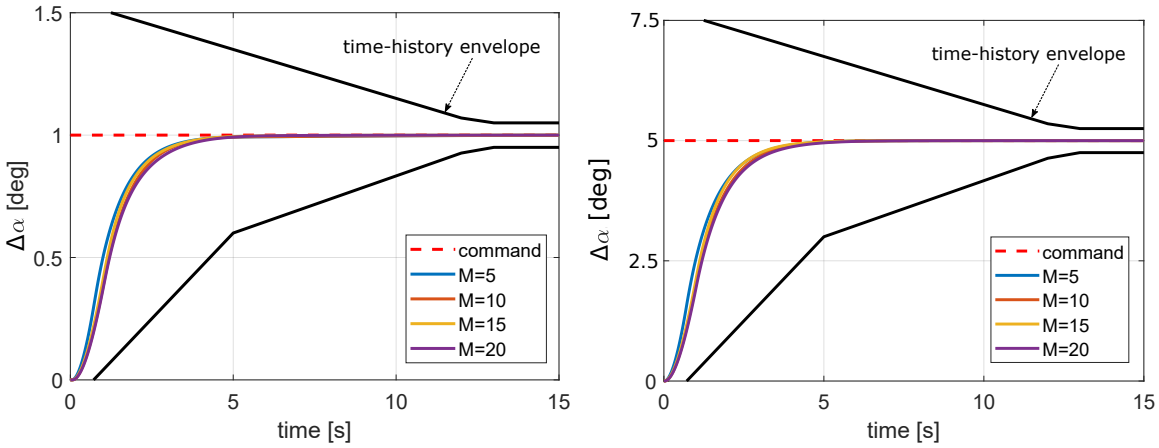

Figure 10: Normalised responses to an angle-of-attack command during FSSC-1 ascent: $\alpha_c = 1°$ (left) and $\alpha_c = 5°$ (right).

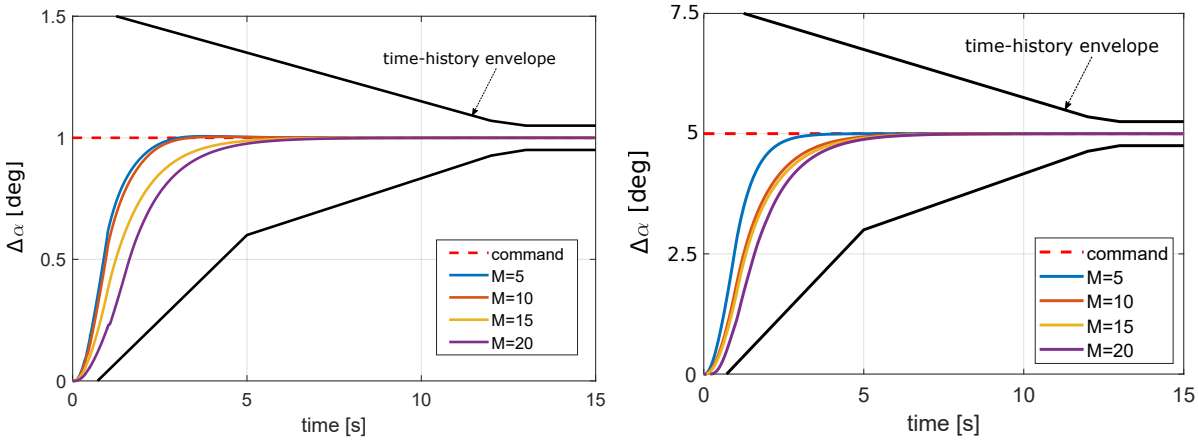

Figure 11: Normalised responses to an angle-of-attack command during FSSC-1 re-entry: $\alpha_c = 1°$ (left) and $\alpha_c = 5°$ (right).

V. Controllability Analysis

A. Response to Attitude Commands

In this section, the capabilities of this control system are studied in relation with the controllability requirements[1,2] The controllability specifications for the longitudinal motion are given as the maximum and minimum values of damping ratio, time rise, settling time, and maximum overshoot of the normalised response to an angle-of-attack step command. So, the normalised transient response of a hypersonic vehicle to an angle-of-attack command shall be graphically bounded by a reference time-history envelope, which is shown in Figs. 10 and 11 by black lines.[8] These plots present the response of the system to 1° and 5° angle-of-attack commands along the ascent and re-entry flight, respectively. The commands are imposed at flight conditions with $M = 5$, 10, 15, 20 along both the ascent and re-entry, defining that the requirements are met for all the design points.

The requirements of controllability along the lateral motion, which are listed in Table 8, are given in terms of time required to realise a 30° bank-angle command. Different from the angle-of-attack commands (step functions), the latter is a ramp, because, when large variations are commanded, the inertia of the system should be taken into account. The results are presented graphically in Fig. 12, where the bank-angle variation $\Delta\sigma$ is plotted as function of time and the rise time is specified. Comparing these results with the

Table 8: Roll-control effectiveness criterion.[13]

Roll Mode	
	Cat. B
Level 1	$t_{30} \leq 4.0$ s
Level 2	$t_{30} \leq 5.0$ s
Level 3	$t_{30} \leq 6.0$ s

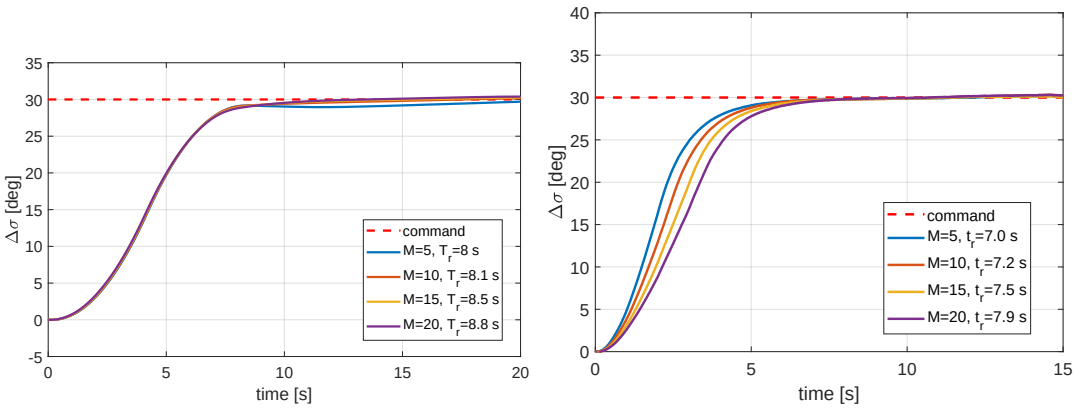

Figure 12: Characteristic responses to a 30° bank command for the ascent (left) and re-entry (right).

requirements, it can be concluded that the system does not meet the MIL requirements along both the ascent and re-entry flight. However, the roll-control effectiveness limits are given as preliminary values to adapt the MIL-Specs to supersonic vehicles. Indeed, the military limits are considered too strict for high-speed vehicles.[13] Thus, it is likely that for hypersonic spaceplanes even more relaxed limits are needed. Overall, it can be concluded that the controller is able to realise the commands so that the desired flight conditions can be reached and the objectives of the mission can be achieved successfully.

An interesting difference between the responses along the ascent and re-entry flight is that the responses at different Mach numbers are almost the same during the ascent, while the higher the Mach number the slower the response during the re-entry. This is essentially due to the different actuators used in these two portions of flight. Along the hypersonic re-entry trajectory, the control surfaces and the RCS thrusters are used to control the vehicle's motion. The control surfaces are strongly dependent on the dynamic pressure, so the effectiveness of the aerodynamic surfaces decreases with decreasing dynamic pressure (i.e., increasing Mach number), resulting in a slower response. Differently, along the ascent trajectory the TVC maintains a high effectiveness along the whole trajectory, since the thrust magnitude is quite large during the whole ascent flight.

Finally, it seems interesting to consider the effect of an error of ±20% of the aerodynamic coefficients on the response to a step command. At the same time, it is desired to compare the performance of the robust and optimal control-system designs in these conditions. It results that the "optimal design" is not able to handle the uncertainty of the aerodynamic data: the final commanded state values are not reached; and the control variables saturate after few seconds. Differently, the robust design can realise the command requiring quite low control effort. Moreover, when a robust control system is integrated into the system, the response remains within the time-history envelope even in the presence of the aerodynamic uncertainty, meeting the controllability requirement.

B. Response to Atmospheric Disturbances

The levels of flying qualities in open-loop and closed-loop studied until now are defined to account for the possibility that the vehicle may operate under off-nominal conditions[1,2]. Abnormalities that may occur

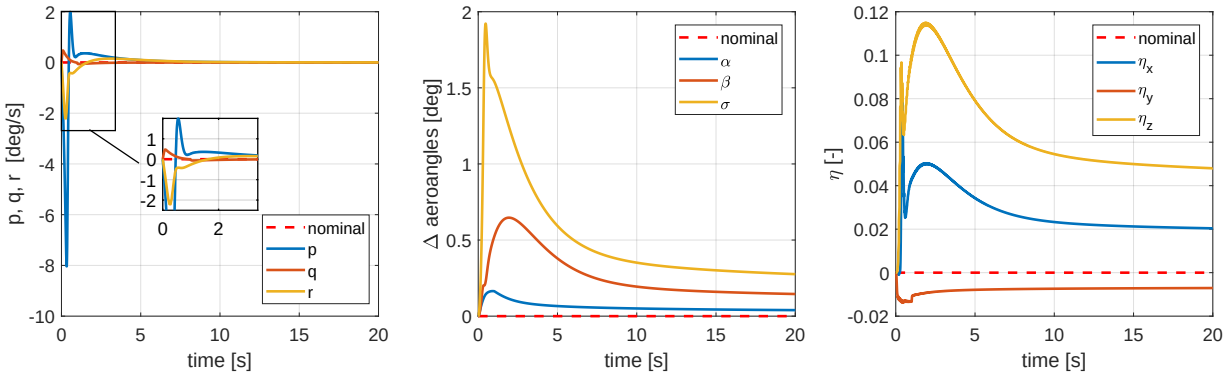

Figure 13: System response to steady state wind ($V_W = 24.8$ m/s) at M = 5 along the re-entry.

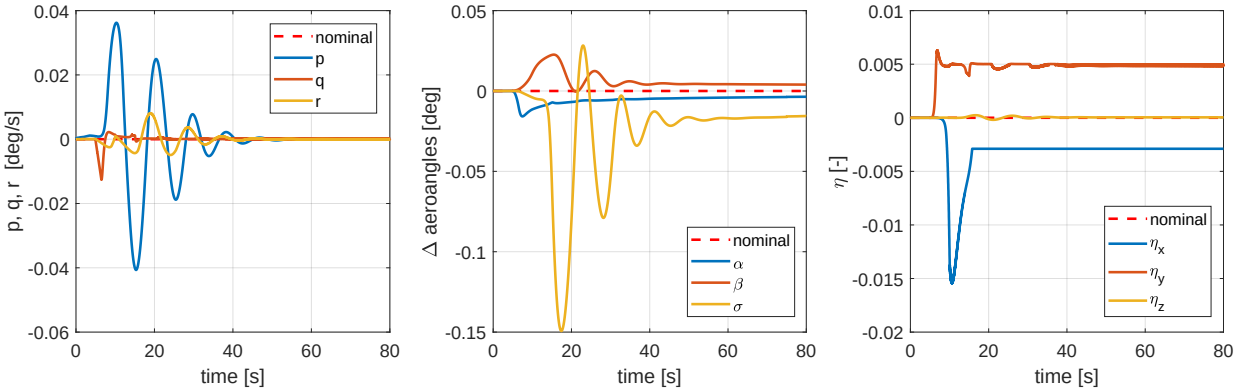

Figure 14: System response to wind gust of magnitude 12 m/s at $M = 15$ along the ascent trajectory.

can be atmospheric disturbances. In this case, a degradation of the flying qualities and controllability characteristics may be allowed. In this section the behaviour of the system in case of atmospheric disturbances is investigated: constant wind, wind gusts, and turbulence. The *horizontal wind model* (HWM07) is used to model steady-state wind, while the wind gusts and turbulence are modelled using the *1-cosine formula* and the *Dryden spectral model*, respectively.

When *steady-state wind* is applied along the hypersonic trajectory of the FSSC-1 spaceplane, it should withstand the disturbance using no more than 75% of the available control authority,[8] i.e., $\eta_{x,y,z_{max}} \leq 0.75$. The wind magnitude and direction angles are computed through the HWM07 on the basis of the position of the vehicle and time epoch expressed in days and seconds. In the following the results are presented only for the design point at $M = 5$ of the re-entry trajectory in Fig. 13. In these points, the wind velocity is $V_W = 24.8$ m/s, which can be classified as *storm* (i.e., level 10 of the Beaufort scale[14]). The system is able to converge to the nominal conditions, using low control power. The moment fractions converge to a steady condition, which is maintained until the wind acts on the vehicle. The MIL-Specs are met also in the other flight conditions. Indeed, the maximum moment fraction required to counteract the effect of steady-state wind and achieve a new stable condition is comprised between 0.01 and 0.15.

The vehicle shall also withstand *wind gusts* with max amplitude of 12 m/s.[8] The wind velocity components are chosen such that it has a total magnitude of 12 m/s and the horizontal and vertical components have the same magnitude, i.e., $V_{w,g} = (6, 6, 8)$ m/s along the x- and y-axes. It is applied at $t = 5$ s. Similarly to what was found for the case of steady-state wind, the system is able to restore equilibrium. The speed of convergence of the response to the new stable conditions varies depending on the flight conditions. For instance, Fig. 14 presents the response to wind gusts at flight condition of $M = 15$ along the ascent, where the stability is obtained at about $t = 60$ s. This value is doubled if we apply the same wind gust at $M = 20$. In addition, we can see that during the ascent the response of the lateral-directional variables oscillates

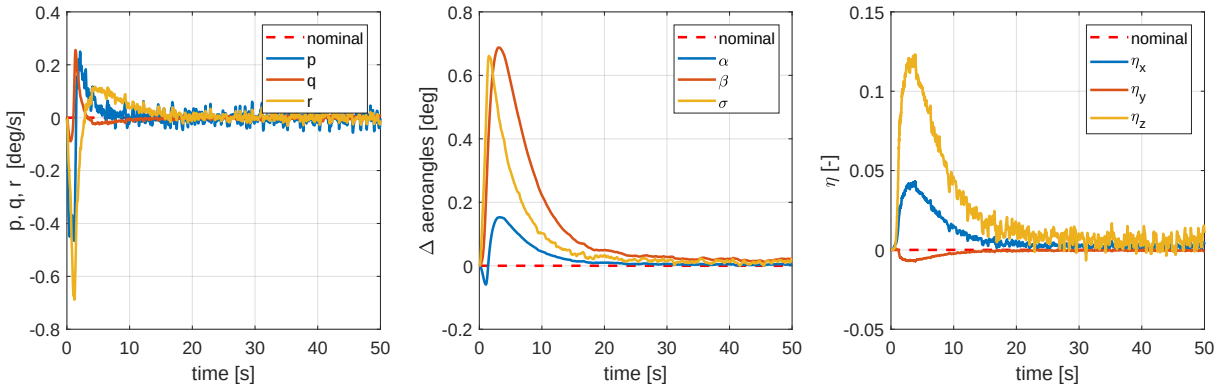

Figure 15: System response to perturbations at $M = 10$ along the re-entry trajectory.

converging to new equilibrium values. This means that a similar perturbation triggers an oscillatory lateral mode of motion of the reference vehicle that ends when the new stable condition is reached. Differently, during re-entry the system behaviour shows proper convergence to the new stable condition.

The response of the system to *turbulence* is presented in Fig. 15 for re-entry flight at $M = 10$. The controller appears to be continuously excited due to the noisy trend that characterises the turbulence. The controller responds to minimise its effect and restore the nominal conditions. The MIL specifications require that the vehicle shall withstand turbulence, modelled with Dryden spectral model, without reaching the control authority limits. That requirement is met both during ascent and re-entry flight, since the maximum moment fraction required is about 0.15. If longer simulations are performed, it can be seen that, although the oscillatory behaviour remains as long as the turbulence acts on the system, the control gains do not saturate.

Overall, some differences between the ascent and re-entry can be highlighted. The state deviations from the nominal conditions and the control required to stabilise the vehicle are generally lower along the ascent trajectory. Indeed, although the points of the trajectory have the same Mach condition, they are characterised by a completely different aerodynamic configuration. Given the strong non-linearity of the aerodynamic properties, the effects that the atmospheric disturbances can have on the vehicle motion are strongly dependent on the flight conditions, especially on α in this particular case. However, during the ascent flight the convergence to the new stable condition seems slower. This can be explained by the fact that the controller is more sensitive and responsive in case of larger deviations from the nominal state.

Also, the higher the Mach number the lower the effect of wind, and the lower is the control effort required to restore a stable condition. Moreover, once the stable condition is reached, it is possible that the aerodynamic angles have a steady-state error with respect to the nominal values. This depends on the accuracy requirement of the controller, which are set by the designer. For control-performance reasons it is suitable to accept 5% error. Furthermore, it is noticed that the actual maximum control power necessary to withstand the atmospheric disturbances is much lower than the requirements defined for subsonic vehicles. This can be linked to the much higher kinetic energy that characterises a hypersonic vehicle. As a consequence, we can deduce that the system can potentially withstand even more severe wind conditions and/or realise attitude commands also in case of off-nominal conditions. It is thus concluded that for the given flight conditions the SAC controller is able to promptly stabilise the vehicle in case of atmospheric disturbances.

VI. Conclusions and Recommendations

The present research has demonstrated that a spaceplane along its hypersonic ascent and re-entry trajectory is characterised by poor flying qualities and stability characteristics. Indeed, the open-loop system does not meet the MIL-requirements. However, when a robust and advanced control system is integrated into the system, the spaceplane becomes stable. A robust design of the controller is developed, by means of a double-loop sensitivity analysis, so that the control system results as insensitive to uncertainties as possible. In this way, the presence of uncertainties can be promptly counteracted and their influence on the performance is minimised.

The response to control commands of the longitudinal motion is generally rated with Level 1 of the MIL-Specs along the ascent and Level 3 along the re-entry. The response to lateral-directional commands does not meet the actual requirements. However, it is likely that these are too strict for hypersonic vehicles and more relaxed limits should be allowed. Also, the system can withstand atmospheric disturbances. Indeed, the controller is able to recover the nominal conditions, stabilising the control variables to a new steady situation and requiring low control effort. This is linked to the high kinetic energy at hypersonic speed that makes the vehicle less sensitive to the effects of the perturbations. It can be concluded that a robust control system is essential for a hypersonic spaceplane to perform a stable flight and achieve the mission objectives.

It could be interesting to perform the analyses of the flying-quality and controllability characteristics throughout the entire ascent and re-entry trajectory. For a full-flight simulation, a guidance system to generate the steering commands needs to be introduced in the simulator. Also, there are some other characteristic manoeuvres in hypersonic missions, such as the cruise flight and a steady-level turn at constant bank angle, where the stability and controllability properties can be studied. Also, the impact of actuators dynamics on the control-system performance and, in addition, how the control system behaves in case of off-nominal situation of the mass distribution (e.g., an offset in the centre-of-mass location), can be further investigated.

References

[1]MIL-F-8785C, "Military Specification Flying Qualities of Piloted Airplanes," *NASA*, 1980.

[2]MIL-HDBK-1797, "Flying Qualities of Piloted Airplanes, Handbook," *Department of Defence, NASA*, 1997.

[3]Cox, T. H. and Jackson, D., "Supersonic Flying Qualities Experience Using SR-71," *NASA*, Technical Memorandum 4800, 1997.

[4]Kaufman, H., Barkana, I. and Sobel, K., "Direct adaptive control algorithms: Theory and applications," Second edition, *Springer-Verlag*, New York, 1998.

[5]Barkana, I. and Guez, A., "Simple adaptive control for a class of non-linear systems with application to robotics," *International Journal of Control*, Vol. 52, No. 1, 1990.

[6]Mooij, E., "Numerical investigation of Model Reference Adaptive Control for hypersonic aircraft," *Journal of Guidance, Control and Dynamics*, vol. 24, no. 2, pp. 315-323, March-April 2001.

[7]Mooij, E., "Simple Adaptive Bank-Reversal Control of a winged Re-entry Vehicle," AIAA-2004-4869, *AIAA Guidance, Navigation, and Control Conference*, Providence, RI, August 16-19, 2004.

[8]Daimler-Benz Aerospace, "FESTIP System Concept Description," *Daimler-Benz Aerospace, ESA*, 1998.

[9]Kuo, B., "Automatic control systems," *Prentice Hall, Inc.*, Englewood Cliffs, New Jersey, 1987.

[10]Mooij, E., "Simple Adaptive Control System Design Trades," AIAA-2017-1502, *AIAA Guidance, Navigation, and Control Conference*, Dallas, TX, January 16-19, 2017.

[11]Mooij, E., "Simple adaptive bank-reversal control for non-linear winged re-entry vehicles", *Mathematics In Engineering, Science And Aerospace*, MESA, Vol. 9, No. 1, pp. 85-110, 2018.

[12]Gopal, M., Modern control system theory, Second Edition, John Wiley & Sons, Inc., Hoboken, NJ, 1993.

[13]Chalk, C. R., "Flying Qualities Design Criteria Applicable to Supersonic Cruise Aircraft," *NASA*, Langley Res. Center Supersonic Cruise Res., pt. 1; pp. 251-267, 1980.

[14]Singleton, F., "The Beaufort scale of winds: its relevance, and its use by sailors," *Weather*, volume 63, no. 2, pp. 37–41, 2008.

[15]Phadke, M. S., "Quality Engineering Using Robust Design," New Jersey, 1989.

[16]MBB, "Study on Re-entry Guidance and Control - Final Report," *Space Communication and Propulsion System*, 1988.

[17]Sachs, G., "Stability and Control Problems in Hypersonic Flight," *Space Course Munich*, 1993.

[18]Mooij, E., "Characteristic Motion of Re-entry Vehicles," AIAA-2013-4603, *AIAA Atmospheric Flight Mechanics* (AFM) Conference, Guidance, Navigation, and Control and Co-located Conferences, American Institute of Aeronautics and Astronautics, 2013.